

# Journal of Materials Chemistry A

Accepted Manuscript

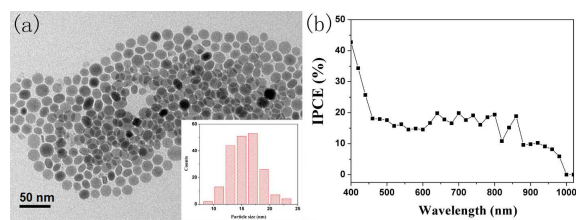


This is an *Accepted Manuscript*, which has been through the Royal Society of Chemistry peer review process and has been accepted for publication.

*Accepted Manuscripts* are published online shortly after acceptance, before technical editing, formatting and proof reading. Using this free service, authors can make their results available to the community, in citable form, before we publish the edited article. We will replace this *Accepted Manuscript* with the edited and formatted *Advance Article* as soon as it is available.

You can find more information about *Accepted Manuscripts* in the [Information for Authors](#).

Please note that technical editing may introduce minor changes to the text and/or graphics, which may alter content. The journal's standard [Terms & Conditions](#) and the [Ethical guidelines](#) still apply. In no event shall the Royal Society of Chemistry be held responsible for any errors or omissions in this *Accepted Manuscript* or any consequences arising from the use of any information it contains.



$\text{Cu}_3\text{SbSe}_3$  nanocrystals have been synthesized for the first time and show excellent photoelectrochemical properties.

Cite this: DOI: 10.1039/c0xx00000x

www.rsc.org/xxxxxx

ARTICLE TYPE

## Colloidal synthesis and characterisation of Cu<sub>3</sub>SbSe<sub>3</sub> nanocrystals

Yike liu<sup>a</sup>, Jia Yang<sup>a</sup>, Ening Gu<sup>a</sup>, Tiantian Cao<sup>c</sup>, Zhenghua Su<sup>a</sup>, Liangxing Jiang<sup>a</sup>, Chang Yan<sup>b</sup>, Xiaojing Hao<sup>b</sup>, Fangyang Liu<sup>\*a</sup> and Yexiang Liu<sup>a</sup>

Received (in XXX, XXX) Xth XXXXXXXXX 20XX, Accepted Xth XXXXXXXXX 20XX

DOI: 10.1039/b000000x

Cu<sub>3</sub>SbSe<sub>3</sub> nanocrystals have been synthesized using hot-injection method. The Cu<sub>3</sub>SbSe<sub>3</sub> nanocrystals possess a band gap of 1.31 eV and the corresponding nanocrystals-electrode shows an incident photon to current efficiency (IPCE) of 10%-35% in the visible region. Our work demonstrates that Cu<sub>3</sub>SbSe<sub>3</sub> nanocrystals have the potential in photo-electric conversion devices application.

Semiconductor nanocrystals are promising candidates in the fields of photovoltaics, thermoelectric, Li-ion batteries and light emitting diodes. Among them, The Cu-V-VI (V = Sb, Bi; VI = S, Se) nano-materials, composed of environmentally benign elements, were considered to be the potential candidates for next-generation solar energy conversion materials and thus this class of the ternary chalcogenides including CuSbS<sub>2</sub>,<sup>1-4</sup> Cu<sub>12</sub>Sb<sub>4</sub>S<sub>13</sub>,<sup>4, 5</sup> Cu<sub>3</sub>SbS<sub>4</sub>,<sup>6</sup> Cu<sub>3</sub>SbS<sub>3</sub>,<sup>7</sup> CuSbSe<sub>2</sub>,<sup>8-10</sup> and Cu<sub>3</sub>BiS<sub>3</sub><sup>11</sup> have received much attention due to their novel properties, earth abundant nature and low cost potential.

Ternary Cu<sub>3</sub>SbSe<sub>3</sub> (CAsE) is an emerging semiconductor.<sup>12</sup> Like other copper-based ternary and quaternary selenides, CAsE has shown excellent thermoelectric properties, which possesses anomalously low thermal conductivity induced by the presence of two additional nonbonding electrons of the Sb<sup>3+</sup> ions.<sup>13-15</sup> Recently, theoretical calculations<sup>16, 17</sup> have demonstrated that the CAsE owns good photovoltaic properties. The CAsE thin film, which displays p-type conductivity behaviour and a direct optical band gap of 1.68 eV, has been synthesized using electrodeposition method by Fernandez and Turner.<sup>18</sup> Maiello et al. used Cu<sub>3</sub>Sb(Se<sub>x</sub>S<sub>1-x</sub>)<sub>3</sub> (CASSE) film to fabricate solar cell devices by two steps synthesis route, obtaining open circuit voltage (V<sub>oc</sub>) and short circuit current density (I<sub>sc</sub>) of 3.5 mV and 1.6 mA cm<sup>-2</sup>, respectively.<sup>19</sup> Owing to its strengths of low cost and non-toxicity, CAsE holds the promise for realising low cost fabrication of thin film solar cells and thermoelectric devices. There are few works on the synthesis of CAsE. CAsE films or bulk materials were reported to be prepared via Cu-Sb or Cu-Sb-Se precursor annealing methods at present.<sup>18, 19</sup> However, to the best of authors' knowledge, there has been no previous report on the synthesis of CAsE nano-materials until now. In order to expand CAsE's application and realize high output roll to roll process, it is of great importance to explore new synthetic methods enabling low cost, large scale and high quality CAsE production. Nanocrystal-ink painting approach is such a technology possessing up-scaling potential for thin film

fabrication, which has been extensively used, especially in the photovoltaic field.<sup>20-25</sup> In this approach, the semiconductor nanocrystals were dispersed in solvents to form a stable nano-ink solution. The nano-ink could then be coated on a substrate using a roll-to-roll method and sintered to form film materials.

In this communication, we firstly reported the synthesis of high quality CAsE nanocrystals by a hot injection method in oleylamine (OLA). A novel highly reactive selenium (Se) precursor was used in the all experiments for the purpose of phosphine-free synthesis of CAsE nanocrystals. It is well known that Se powder is difficult to dissolve in OLA to form a reactive precursor on its own. But it has recently been reported that Se powder can be dissolved in the presence of OLA via phase transfer protocol.<sup>26, 27</sup> In this protocol, Se was first reduced by sodium borohydride (NaBH<sub>4</sub>) or dodecanethiol (DT) into low valence Se, which further associates with OLA to form OLA<sub>m</sub>Se<sub>n</sub>, thus making the element Se soluble. However NaBH<sub>4</sub> is easily oxidized in the open air, and its reduction by NaBH<sub>4</sub> must be assisted with ultrasonication. Besides, DT is unstable at high synthesis temperature, which would introduce elemental sulphur due to DT decomposition during the synthesis process. In contrast, dimethylamine borane (DMAB) is a more stable reducing reagent. Herein DMAB was employed to facilitate the dissolution of Se powder in OLA. Se was first reduced by DMAB to generate an alkylammonium selenide at 110 °C, which could then be dissolved in OLA to form a bright-yellow color solution. This Se precursor is highly reactive and suitable for the synthesis of CAsE nanocrystals. The necessary conditions to synthesize phase pure nanocrystals with narrow size distribution are discussed and corresponding growth process is preliminarily investigated. The synthesized nanocrystals have the diameters in the range from about 13 nm to 18 nm and an optical band gap of 1.31 eV. These nanocrystals can be easily dispersed in a comparably low-toxic solvent to form a stable ink, and then the CAsE film can be readily fabricated using the developed ink by drop casting method. The obtained films demonstrate a clear photoresponse, showing that CAsE thin films synthesized from its nanocrystals have the potential in the application of photo-electric conversion devices.

The syntheses of CAsE nanocrystals were carried out utilizing a hot-injection method via a standard air-inert Schlenk line. In a typical synthesis, Se powder was dissolved in OLA completely with the assistance of DMAB as co-solvent at 110 °C, obtaining a Se/DMAB/OLA solution with bright-yellow color. Then the

Se/DMAB/OLA solution was quickly injected into the hot solution of OLA containing stoichiometric amount of copper (II) acetylacetonate and antimony (III) acetate [atom ratio Cu: Sb = 3:1] at 190 °C for 30 min under Ar atmosphere. Full experimental details can be found in the Supporting Information (ESI†). Fig. 1 demonstrates basic structural characterization of synthesized nanocrystals. They are round shaped nanocrystals with an average diameter of  $15.7 \pm 2.7$  nm as indicated in the low-magnification TEM image (Fig. 1a). The corresponding size distribution chart is given as an inset in Fig. 1a (additional TEM images can be found in the ESI† Fig. S1). A high-resolution TEM (HRTEM) image (Fig. 1b) shows a clear crystalline surface with the interplanar spacing of 1.95, 2.00 and 2.32 Å corresponding to the (322), (400) and (222) planes of CAsE, respectively, demonstrating the nano-scale evidence that the synthesized nanocrystals possess the structure of CAsE. The lattice data calculated from selected area electron diffraction (SAED) pattern of randomly chosen region of CAsE nanocrystals agrees well with the lattice parameters of CAsE (Fig. 1c).

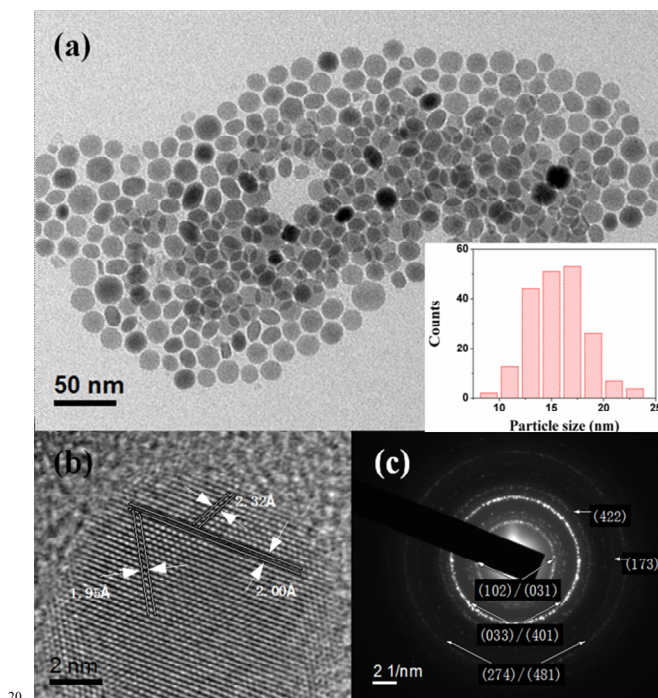


Fig. 1 (a) Low resolution TEM image of CAsE nanocrystals. (b) High resolution TEM image showing interplanar spacing of 1.95 Å, 2.00 Å and 2.32 Å. (c) The SAED pattern indexed to CAsE.

Fig. 2 illustrates the X-ray diffraction (XRD) pattern of the prepared nanocrystal. All the diffraction peaks can be readily indexed to the orthorhombic phase (Pnma) of CAsE (JCPDS no. 86-1751). No evidence of other impurities such as  $\text{Cu}_2\text{Se}$  (JCPDS no. 65-2982),  $\text{CuSbSe}_2$  (JCPDS no. 75-0992), etc., can be found from the XRD pattern. The element composition of synthesized CAsE nanocrystals estimated by Energy Dispersive X-ray spectroscopy (EDS) is  $\text{Cu}_{2.98}\text{SbSe}_{3.09}$  (See ESI† Fig. S2), which is close to the stoichiometric composition of CAsE.

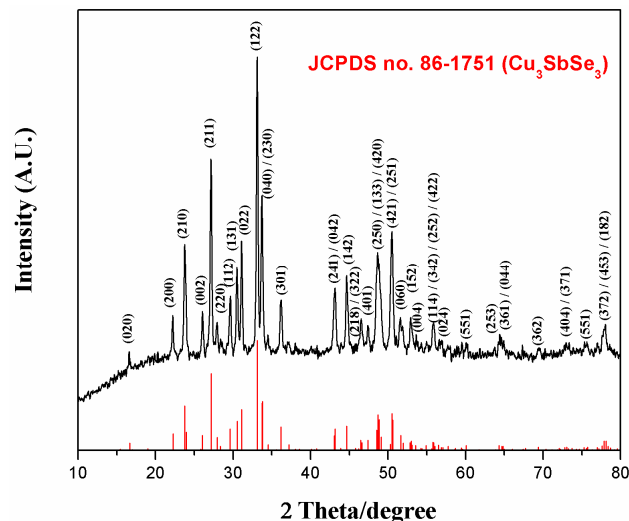


Fig. 2 XRD pattern of CAsE nanocrystals [Cu  $\text{K}\alpha$  radiation ( $\lambda = 1.54$  Å)]. The reference pattern is standard tetragonal CAsE (JCPDS no. 86-1751)

The composition and valence states of the CAsE nanocrystals were further investigated by XPS. As shown in Fig. 3, the binding energies of Cu 2p, Sb 3d, and Se 3d of the nanocrystals in the XPS are consistent with those reported in literatures.<sup>7, 28, 29</sup> The valence states of Cu, Sb, and Se ions are +1, +3, and -2, respectively. The composition determined from XPS is also close to the stoichiometric composition of CAsE, agreeing well with the EDS result.

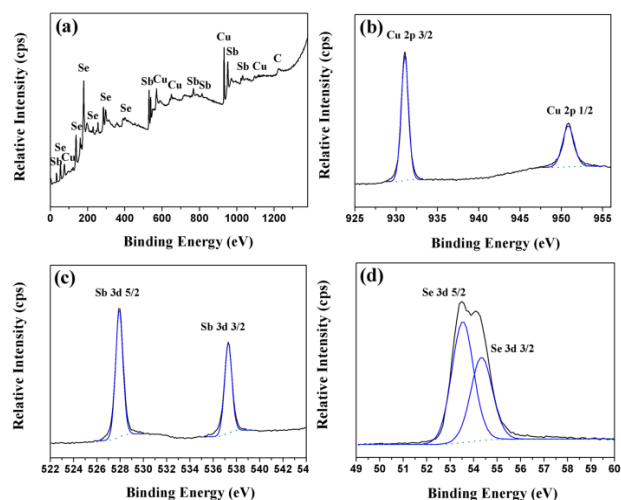


Fig. 3 XPS spectra of CAsE nanocrystals. (a) The full Scan spectrum. (b) Cu 2p spectrum. (c) Sb 3d spectrum. (d) Se 3d spectrum. The fits are also shown. (blue lines)

Besides, we investigated the effect of precursor ratios and found they play a key role in the synthesis process (XRD patterns for synthesized product at different ratios of precursors were given in the ESI† Fig. S3). Considering elemental ratio Cu:Sb of 3:1 in CAsE, a stoichiometric of 3-fold excess of copper over antimony (Cu:Sb=3:1) was applied in all experiments. The formation of pure CAsE was found to be highly dependent on the content of Se precursor. During a series of trial reactions, the amount of injection Se was varied. For mole ratios of metal (Cu+Sb) to Se within the range of 4:3 to 4:4, the CAsE phase was

produced while both  $\text{CuSbSe}_2$  (JCPDS no. 75-0992) and  $\text{Cu}_2\text{Se}$  (JCPDS no. 65-2982) were detected simultaneously. Interestingly, with the increase of content of Se, peaks assigned to  $\text{CuSbSe}_2$  and  $\text{Cu}_2\text{Se}$  gradually disappeared. Pure CAsE can be obtained when (Cu+Sb): Se ratio was 4:4. In addition, the use of excess Se was found to be necessary to balance relativity of cationic precursors to avoid the side reactions and the formation of impurities. A similar synthetic strategy has also been previously reported and used for synthesis of I-III-VI semiconductor nanocrystals via hot-injection method.<sup>28, 30, 31</sup>

To explore the possible pathway for the formation of CAsE nanocrystals, the phase data of the reaction products upon different reaction time were studied by XRD (See ESI† Fig. S4). In the initial stage (1 min), CAsE phase has already been formed, indicating that the Se precursor has high reactivity, and thereby facilitates the reaction between Cu, Sb and Se simultaneously. No other impurities phase, such as  $\text{CuSe}$ ,  $\text{Cu}_2\text{Se}$ , and  $\text{CuSbSe}_2$  were detected in the XRD pattern, which suggests that the synthesis of CAsE nanocrystals should be one-step process. With the reaction time proceeded to 4 min, 8 min, 16 min and 32 min, according to XRD, the main phase of CAsE remained unchanged. However, when the reaction time was reached 64 min, peaks assigned to  $\text{Cu}_3\text{SbSe}_4$  (JCPDS no. 25-0263) were detected, which might result from the further reaction between CAsE nanocrystals and excess Se.

In addition, experiments at different reaction (injection) temperatures have been trialled. As shown in ESI† Fig. S5-6, at the relative low temperature, such as 160 °C, 190 °C and 220 °C, the products are pure CAsE. The optimum reaction temperature of the reaction is found to be around 190 °C. When the temperature was elevated to 220 °C, NCs showed slight aggregation. While at 160 °C, the rate of the reaction decreased and nonuniform nanocrystals were obtained. When the synthesis temperatures are raised above 250 °C,  $\text{CuSbSe}_2$  was detected in addition to the desired phase CAsE nanocrystals.

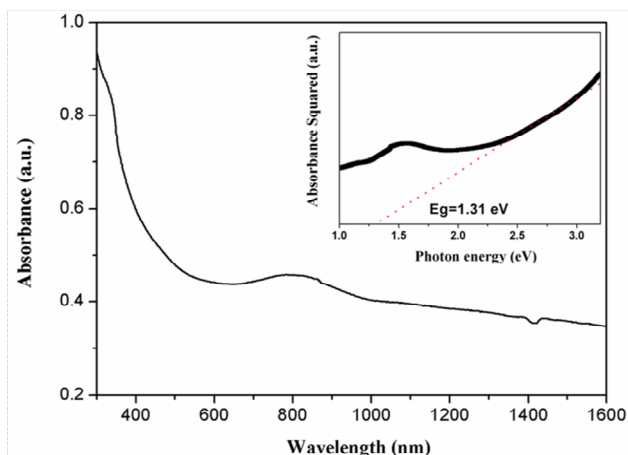


Fig. 4 UV-vis-NIR absorption spectrum of the as-synthesized nanocrystals. Inset shows the  $\text{abs}^2$  vs.  $\text{eV}$  for the CAsE nanocrystals; the estimated band energy is 1.31 eV.

The absorption spectrum of as-synthesized CAsE nanocrystals was measured using UV-vis-NIR absorbance spectroscopy (See Fig. 4). The band gap of the CAsE nanocrystals is estimated to be 1.31 eV by extrapolating the linear region of the plot of the

absorbance squared versus energy, as shown in the inset of Fig. 4. The value is close to the optimal value for solar cell application.<sup>32</sup> In addition, a broad band that extends from around 700 nm to the NIR region is observed. The origin of this band needs to be further explored in the future work.

To test the photoresponse of CAsE nanocrystals, thin film of the nanocrystals was drop-casted onto ITO substrate. This film was mounted to a custom-built three-electrode photoelectrochemical cell with a graphite counter electrode and saturated calomel reference electrode (SCE) containing 0.5 M  $\text{H}_2\text{SO}_4$ . In general, photoelectrochemical (PEC) is an excellent tool to assess the photovoltaic performance of new light-absorber materials. This method is popular because it could reduce the recombination probability of minority carriers with photogenerated holes and provide nearly ideal contact to the half cell, avoiding problems such as interface contact and lattice matching with the full device architecture.<sup>11, 33</sup>

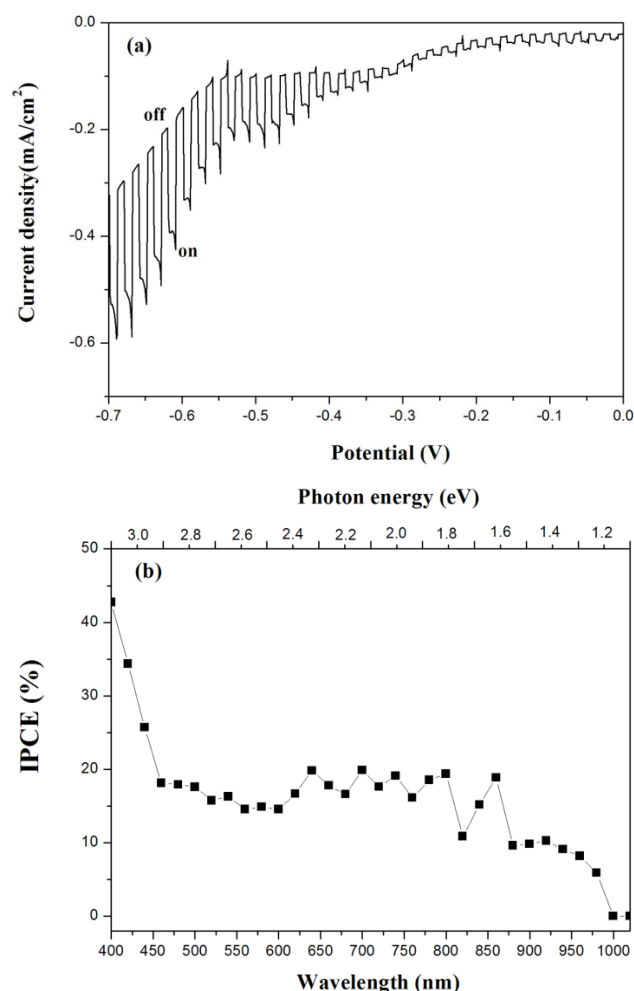


Fig. 5 Photocurrent-potential plot of the CAsE films on an ITO substrate in 0.5 M  $\text{H}_2\text{SO}_4$  under  $100 \text{ mW cm}^{-2}$  illumination. The inset shows the transient photocurrent spectrum at -0.65 V vs. SCE.

Fig. 5(a) displays the current density versus potential (vs SCE) plots for the prepared CAsE films utilizing chopping method (40 s light on, 40 s light off). The photocurrent density increases with negative shift of the cathodic potential, which is the typical character of p-type semiconductor for CAsE nanocrystals film.<sup>27</sup>

In this case, electrons are transferred from the conduction band to the oxidant in solution, and then from the back contact (here ITO) into the semiconductor, leading to the observed reductive current. The photocurrent density reaches a saturated value of about 0.22 mA cm<sup>-2</sup> at -0.65V vs. SCE. The transient photocurrent at this voltage is obtained (see ESI† Fig. S7), showing excellent photoresponse characteristics and good photostability of nanoink casting CAsE film over many cycles (12 cycles demonstrated here). The magnitude of the gained photoresponse is high enough to acquire the IPCE spectrum, as show in Fig. 5(b). Approximately 10%-35% of the incident photons can be readily converted to electron and hole pairs in the wavelength region of 400-980 nm that covers most of the visible spectrum. The IPCE of CAsE is higher than that of the others Cu-V-VI semiconductor materials<sup>1, 10</sup> in the entire absorption region. The IPCE value reaches zero when the photon energy goes below 1.24 eV, which corresponds to the band gap of synthesized CAsE and agrees well with the value estimated from the UV-vis-NIR data.

## Conclusions

In summary, a colloidal synthesis of CAsE nanocrystals via the hot-injection method is presented by utilizing a high reactivity phosphine-free Se precursor. The structure of the synthesized CAsE nanocrystals is confirmed simultaneously by high-resolution TEM image, SAED pattern and XRD. The results of EDS and XPS confirmed the composition of the CAsE nanocrystals. Both the ratios of precursors and temperature play a crucial role in determining the phase and shape of the synthesised nanocrystals. CAsE nanocrystals could be formed in a short period of time owing to the high reactivity of Se precursor. A band gap of 1.31 eV for CAsE nanocrystals is estimated by UV-vis-NIR data. The CAsE nanocrystals film yields an excellent photoresponse in PEC tests and an IPCE of 10%-35% in the visible region. Our work demonstrates that the synthesized CAsE nanocrystals have potential in the field of photo-electric conversion devices application. Our future work will focus on the utilization of CAsE nanocrystals for the development of full photovoltaic devices.

## Acknowledgements

This work was supported by the National Natural Science Foundation of China (Grant No. 51222403) and China Postdoctoral Science Foundation (Grant No. 2012M511403 and 2013T60777).

## Notes and references

<sup>a</sup> School of Metallurgy and Environment, Central South University, Changsha 410083, China. E-mail: liufangyang@csu.edu.cn

<sup>b</sup> School of Photovoltaic and Renewable Energy Engineering, University of New South Wales, Sydney, NSW 2052, Australia

<sup>c</sup> Institute Of Nuclear And New Energy Technology, Tsinghua University, Beijing, 100084, China

† Electronic Supplementary Information (ESI) available: [details of any supplementary information available should be included here]. See DOI: 10.1039/b000000x/

‡ Footnotes should appear here. These might include comments relevant to but not central to the matter under discussion, limited experimental and spectral data, and crystallographic data.

1. C. Yan, Z. Su, E. Gu, T. Cao, J. Yang, J. Liu, F. Liu, Y. Lai, J. Li and Y. Liu, *RSC Advances*, 2012, 2, 10481-10484.
2. A. Rabhi and M. Kanzari, *Chalcogenide Letters*, 2011, 8, 255-262.
3. W. Septina, S. Ikeda, Y. Iga, T. Harada and M. Matsumura, *Thin Solid Films*, 2014, 550, 700-704.
4. D. Xu, S. Shen, Y. Zhang, H. Gu and Q. Wang, *Inorganic Chemistry*, 2013, 52, 12958-12962.
5. J. van Embden, K. Latham, N. W. Duffy and Y. Tachibana, *Journal of the American Chemical Society*, 2013, 135, 11562-11571.
6. J. van Embden and Y. Tachibana, *Journal of Materials Chemistry*, 2012, 22, 11466-11469.
7. X. Qiu, S. Ji, C. Chen, G. Liu and C. Ye, *CrystEngComm*, 2013, 15, 10431-10434.
8. D. Tang, J. Yang, F. Liu, Y. Lai, M. Jia, J. Li and Y. Liu, *Electrochemical and Solid-State Letters*, 2011, 15, D11-D13.
9. D. Colombara, L. M. Peter, K. Rogers, J. Painter and S. Roncallo, *Thin Solid Films*, 2011, 519, 7438-7443.
10. D. Tang, J. Yang, F. Liu, Y. Lai, J. Li and Y. Liu, *Electrochimica Acta*, 2012, 76, 480-486.
11. C. Yan, E. Gu, F. Liu, Y. Lai, J. Li and Y. Liu, *Nanoscale*, 2013, 5, 1789-1792.
12. A. Pfitzner, *Zeitschrift für anorganische und allgemeine Chemie*, 1995, 621, 685-688.
13. C. Sevik and T. Cagin, *Journal of Applied Physics*, 2011, 109, 123712.
14. E. J. Skoug, J. D. Cain and D. T. Morelli, *Applied Physics Letters*, 2010, 96, 181905.
15. Y. Zhang, E. Skoug, J. Cain, V. Ozoliņš, D. Morelli and C. Wolverton, *Physical Review B*, 2012, 85, 054306.
16. L. Yu, R. S. Kokenyesi, D. A. Keszler and A. Zunger, *Advanced Energy Materials*, 2013, 3, 43-48.
17. A. B. Kehoe, D. J. Temple, G. W. Watson and D. O. Scanlon, *Physical Chemistry Chemical Physics*, 2013, DOI: 10.1039/C3CP52482E, 15477-15484.
18. A. M. Fernández and J. A. Turner, *Solar Energy Materials and Solar Cells*, 2003, 79, 391-399.
19. Pietro Maiello, Guillaume Zoppi, Robert W. Miles, Nicola Pearsall and I. Forbes, *Solar Energy Materials and Solar Cells*, 2013, 113, 186-194.
20. Q. Guo, G. M. Ford, W.-C. Yang, B. C. Walker, E. A. Stach, H. W. Hillhouse and R. Agrawal, *Journal of the American Chemical Society*, 2010, 132, 17384-17386.
21. Q. Guo, H. W. Hillhouse and R. Agrawal, *Journal of the American Chemical Society*, 2009, 131, 11672-11673.
22. Q. Guo, S. J. Kim, M. Kar, W. N. Shafarman, R. W. Birkmire, E. A. Stach, R. Agrawal and H. W. Hillhouse, *Nano Letters*, 2008, 8, 2982-2987.
23. S. Peng, S. Zhang, S. G. Mhaisalkar and S. Ramakrishna, *Physical Chemistry Chemical Physics*, 2012, 14, 8523-8529.
24. M. G. Panthani, V. Akhavan, B. Goodfellow, J. P. Schmidtke, L. Dunn, A. Dodabalapur, P. F. Barbara and B. A. Korgel, *Journal of the American Chemical Society*, 2008, 130, 16770-16777.
25. J. Puthussery, S. Seefeld, N. Berry, M. Gibbs and M. Law, *Journal of the American Chemical Society*, 2010, 133, 716-719.

- 
26. Y. Wei, J. Yang, A. W. H. Lin and J. Y. Ying, *Chemistry of Materials*, 2010, 22, 5672-5677.
27. Y. Liu, D. Yao, L. Shen, H. Zhang, X. Zhang and B. Yang, *Journal of the American Chemical Society*, 2012, 134, 7207-7210.
- 5 28. H. Zhong, Y. Li, M. Ye, Z. Zhu, Y. Zhou, C. Yang and Y. Li, *Nanotechnology*, 2007, 18, 1-6.
29. H. Chen, S.-M. Yu, D.-W. Shin and J.-B. Yoo, *Nanoscale research letters*, 2010, 5, 217-223.
30. R. Xie, M. Rutherford and X. Peng, *Journal of the American Chemical Society*, 2009, 131, 5691-5697.
- 10 31. M. J. Thompson, T. P. A. Ruberu, K. J. Blakeney, K. V. Torres, P. S. Dilsaver and J. Vela, *The Journal of Physical Chemistry Letters*, 2013, DOI: 10.1021/jz402048p, 3918-3923.
32. A. Goetzberger, C. Hebling and H. W. Schock, *Mat Sci Eng R*, 2003,
- 15 40, 1-46.
33. H. Ye, H. S. Park, V. A. Akhavan, B. W. Goodfellow, M. G. Panthani, B. A. Korgel and A. J. Bard, *The Journal of Physical Chemistry C*, 2010, 115, 234-240.

20